JES Focus Issue on Oxygen Reduction and Evolution Reactions for High Temperature Energy Conversion and Storage

Insight into the Reaction Mechanism of $(La_{0.58}Sr_{0.40})(Co_{0.20}Fe_{0.80})O_{3-\delta}$ Cathode with Volatile Chromium Species at High Current Density in a Solid Oxide Fuel Cell Stack

Alexander Beez,[a,b,z] Xiaoyan Yin,[c] Norbert H. Menzler,[b,*] Robert Spatschek,[c] and Martin Bram[a,b]

[a] *Christian Doppler Laboratory for Interfaces in Metal-Supported Electrochemical Energy Converters, 52425 Jülich, Germany*
[b] *Forschungszentrum Jülich, Institute of Energy and Climate Research, IEK-1: Materials Synthesis and Processing, 52425 Jülich, Germany*
[c] *Forschungszentrum Jülich, Institute of Energy and Climate Research, IEK-2: Microstructure and Properties of Materials, 52425 Jülich, Germany*

Anode-supported solid oxide fuel cells with different Cr protection layers on the metallic interconnect were operated in a short stack at 700°C for 1240 h. The current density was raised sequentially from 0.5 A cm^{-2} during the first 240 h of operation to 0.75 A cm^{-2} for a further 1000 h. After operation, the (La,Sr)(Co,Fe)$O_{3-\delta}$ (LSCF) cathode layers were analyzed with respect to Cr interaction by both wet chemical and microstructural methods. For cells equipped with interconnects coated with a dense APS protection layer, the amount of Cr on the cathode was in the range of a few µg. For cells with a porous WPS coating on the interconnect, the amount of Cr was in the range of 110–160 µg cm^{-2} and Cr-containing phases were detected by SEM analysis both on top of the cathode layer and also at the LSCF/GDC interface, which has rarely been observed before. In addition, a deterioration of the cathode microstructure near the LSCF/GDC interface was observed. With respect to the high current density during operation, a theory was developed which explains both the Cr deposition at the LSCF/GDC interface and also the deterioration of the cathode.

Manuscript submitted April 20, 2017; revised manuscript received May 23, 2017. Published June 13, 2017. *This paper is part of the JES Focus Issue on Oxygen Reduction and Evolution Reactions for High Temperature Energy Conversion and Storage.*

Climate change, limitation of resources, technical and political obstacles associated with nuclear power and changes in the global energy economy are only a few reasons why the world needs alternative concepts for its future energy supply. One key technology offering decentralized energy supply is solid oxide fuel cells (SOFC).[1] Their high efficiency; fuel flexibility and scalability allows them to be used as decentralized power plants or, on a smaller scale, in auxiliary power units or range extenders in mobile applications.[2–4]

During the development and optimization of SOFC stacks and systems, attention was not only focused on performance but also on the application of cost-efficient materials. One major improvement was the establishment of metallic interconnects, offering high electronic and thermal conductivity and mechanical stability while also decreasing the price per repeating unit compared to full ceramic stack designs.[5] However, the preferentially used Cr-containing steels lead to pronounced performance degradation due to the evaporation of Cr compounds, which then react with the cathode. Under the oxidizing conditions on the cathode side, hexavalent Cr species such as CrO_3 and $CrO_2(OH)_2$ evaporate from the oxide scale of the interconnect or balance-of-plant components and react with the LSCF cathode material to form a Sr- and Cr-containing oxide scale thereby decreasing cell performance.[3,6,7] This effect is known to be influenced by parameters such as Cr partial pressure, air humidity and temperature.[8–10] To avoid this Cr-related degradation, different strategies have been developed to either reduce the Cr partial pressure to an acceptable level for the desired operating time or to increase the Cr tolerance of the cathode material itself. The most promising technique for avoiding Cr poisoning is to coat the interconnect steel with a preferentially dense protection layer. This layer either prevents the Cr scale coming into contact with the gas phase or serves as a Cr getter by offering a reaction partner to form a more stable product phase thereby decreasing the Cr partial pressure in the cathode compartment.[11,12] In particular, dense layers applied by atmospheric plasma spraying (APS) have proven able to reduce the Cr deposition on the cathode and thereby considerably lessen degradation.[13–16] However, even with the most effective protective coatings Cr cannot be completely prevented from entering the gas phase and finally reacting with the cathode material. Uncoated balance-of-plant components are an almost unavoidable source of volatile Cr species under SOFC operating conditions.

During cathode development, mixed-conducting perovskite cathode materials such as (La,Sr)(Co,Fe)$O_{3-\delta}$ (LSCF) have been proven to deliver high cell performance over a long operating time. However, due to the segregation of Sr they are prone to Cr-related degradation.[17] Many perovskite materials, including common SOFC cathodes such as LSC, LSCF and LSM ((La,Sr)MnO_3), display this segregation of Sr from the perovskite lattice to the surface.[18–20] It is driven by high temperature and mechanical stress[21,22] as well as by relaxation of crystal defects.[23] The Sr from the perovskite lattice forms SrO crystals on the entire available cathode surface, which is a possible reaction partner for volatile Cr species. For LSCF cathodes, the degradation product is often found under the channels of the flow field.[9,24,25] The most widespread theory describing the reaction of gaseous Cr with Sr-containing cathodes such as LSCF is the nucleation theory.[9] It is based on a chemical reaction of the Cr species in the gas phase with segregated SrO on the cathode surface, which is kinetically fast and results in the formation of Sr-Cr-(O)-nuclei (1). The further reaction with more Cr from the gas phase and SrO from the cathode surface results in the growth of an insulating $SrCrO_4$ oxide scale (2).

$$Cr O_{3(g)} + Sr O_{(s)} \rightarrow Cr - Sr - O_{(nuclei)(s)} \quad [1]$$

$$Cr - Sr - O_{(nuclei)(s)} + Cr O_{3(g)} + Sr O_{(s)} \rightarrow Sr Cr O_{4\,(s)} \quad [2]$$

This reaction behavior is supported by experimental findings with and without polarization, where Cr is detected on the surface of the cathode.[9,26,27] However, there is evidence that the degradation behavior of LSCF is more complex than the nucleation theory predicts. In a previous stack test, we showed that after 2500 h of operation Cr species can also be found at the LSCF/GDC interface in an ASC stack using a thin-film 8 mol-% yttrium-stabilized zirconia electrolyte

*Electrochemical Society Member.
[z] E-mail: a.beez@fz-juelich.de

Table I. Distribution of the interconnect coatings in the stack.

Layer number	Interconnect coating	Position
4	APS / MCF	Top
3	WPS / MnO_x	↑
2	APS / MCF	
1	WPS / MnO_x	Bottom

(8YSZ) prepared by sol-gel technology and a physical vapor-deposited barrier layer.[28] Compared to state-of-the-art cells with screen-printed GDC diffusion barrier and 8YSZ electrolyte, the ionically conducting layers in this stack are only 2 μm (1 μm GDC + 1 μm 8YSZ; GDC: gadolinia-doped ceria) instead of approximately 15 μm (5 μm GDC + 10 μm 8YSZ). With the stack test presented here, we seek to provide insights into the degradation behavior of LSCF cathodes operated under high load conditions, which also seems to enable additional reactions. The findings and the conclusions drawn about this approach could complement current knowledge on SOFC degradation processes using LSCF-based cathodes.

Experimental

Stack description.—For this work, a JUELICH F-Design short stack with four layers and conventional anode-supported SOFCs was operated. The anode was screen printed on a ∼500 μm thick anode support (NiO Mallinckrodt Baker, Germany; 8YSZ UCM Ceramics, Germany) prepared by tape casting and pre-sintered at 1230°C. The NiO/8YSZ composite anode (NiO Mallinckrodt Baker, Germany; 8YSZ Tosoh, Japan) had a thickness of ∼7 μm. On this, the 10 μm thick 8YSZ electrolyte (8YSZ Tosoh, Japan), a 5 μm thick GDC (Treibacher, Austria) diffusion barrier layer and a 40 μm LSCF cathode were applied and sintered at 1400, 1300 and 1080°C, respectively. The cathode had a composition of $(La_{0.58}Sr_{0.40})(Co_{0.20}Fe_{0.80})O_{3-\delta}$ and was produced in-house by spray drying and calcination. To ensure good electrical contact between the ASC and the interconnect, a nickel mesh was used on the anode side. On the cathode side, a perovskite containing lanthanum, cobalt, copper and manganese with high electrical conductivity was applied by screen printing. This cathode contact layer (LCC10) was also produced in-house. The sealant of the stack was a glass ceramic (glass 87 ZYBF-2).[29] As a sealing procedure, the stack was kept at 850°C for 100 h, followed by reduction of the anode by enhancing the hydrogen flux. Further information about the stack design and joining can be found in Ref. 15.

Crofer22APU (ThyssenKrupp, Germany) was used as the interconnect. In contrast to standard stack tests, the interconnects were not coated uniformly in the complete stack. Every other layer was coated with MnO_x via wet powder spraying (WPS) and a $(Mn)(Co_{1.9}Fe_{0.1})O_4$ spinel (MCF) via atmospheric plasma spraying (APS). Table I gives an overview of the position of the layers with different coatings in the assembled stack.

One major difference between these two protective coatings is their respective density. As shown in Fig. 1, the coating prepared by APS is quite dense. The middle of the layer and the MCF/Crofer22APU interface show an apparent porosity which is a known issue from sample preparation and is not related to the layer deposition or stack operation. The higher magnification in Fig. 1b shows the high density of the MCF layer prepared by APS. In comparison, the MnO_x layer prepared by WPS remains rather porous. In addition, the layer is thinner by a factor of 2–3 compared to the APS protection coating.

Due to the different materials and microstructures, interaction with Cr species is different for the two types of protection layers. The APS coating protects the underlying cell by acting as a diffusion barrier layer for the chromium, while the WPS coating serves as a Cr getter, reacting with volatile Cr species from the gas phase and forming a Cr-Mn-spinel. The Cr partial pressure above such a spinel phase is lower compared to metallic interconnects forming an intrinsically pure Cr_2O_3 layer.[30–32]

Stack operation.—The stack was operated in a furnace to achieve low thermal gradients over the stack. The set-point of the furnace was 700°C while the measured furnace temperature increased to 725°C when load operation of the stack began. During operation, the stack was fed with hydrogen containing 20% water vapor on the anode side and with dry, synthetic air on the cathode side. Fuel and air utilization amounted to 40%. The stack was in operation for about 1500 h at 700°C (1250 h under load). Fig. 2 summarizes the operating curves as well as the U-I-curves before and after operation.

For the first 240 h of operation, the current density was 0.5 A cm^{-2} and it was raised to 0.75 A cm^{-2} for the last 1000 h. The increase of the current density resulted in an increase of the average stack temperature from 730°C to 745°C.

After operation the stack was cooled down and dismantled. Parts of different layers were separated by laser cutting.[33] To measure the amount of Cr per cathode surface area, the cathode layers were removed from some of the samples by chemical etching with perchloric acid. The solution was analyzed by inductively coupled plasma-optical impedance spectroscopy (ICP-OES). The remaining samples were either prepared for surface imaging or embedded in resin and polished for cross sectional SEM imaging. An FEG-SEM Ultra 55 (Zeiss, Germany) was used for the microstructural analysis.

Results

Performance degradation.—According to the operating curves presented in Fig. 2, there is a noticeable difference in degradation depending on the interconnect coating of the respective layer. While the layers with APS coatings on the interconnect decrease moderately at a fixed rate, the layers with WPS coating show a much more pronounced progressive degradation. Before stack shutdown, the voltage degradation reached 2–5% and 12–17% for the layers with APS and WPS protection coatings, respectively. The higher degradation of layer 1 can be attributed to the position inside the stack. This behavior is often observed for the bottom layer of an SOFC stack and is attributed to lower heat transfer, as the only heat input from below is delivered by the furnace. As a result, the bottom layer delivers a lower cell voltage at a fixed current density and tends to degrade more strongly than the cells from the layers above. Apart from the increased degradation rate, the trend of the degradation process of layer 1 is quite similar to layer 3, which also has an interconnect coating prepared by WPS.

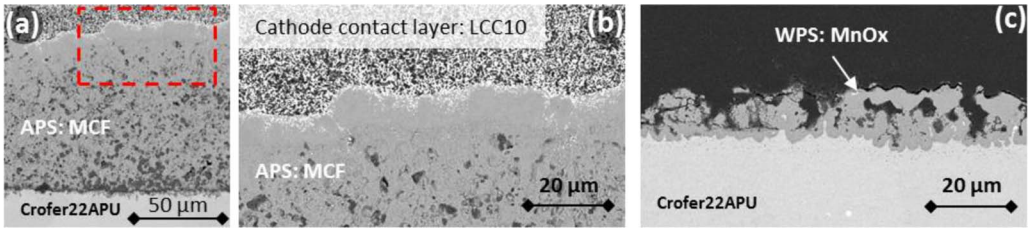

Figure 1. Comparison between the APS (layer 4) and WPS (layer 1) interconnect coating.(a) Overview of the APS coating with breakouts due to sample preparation; (b) area marked in red from (a) showing the dense structure of the APS layer; (c) highly porous MnO_x coating.

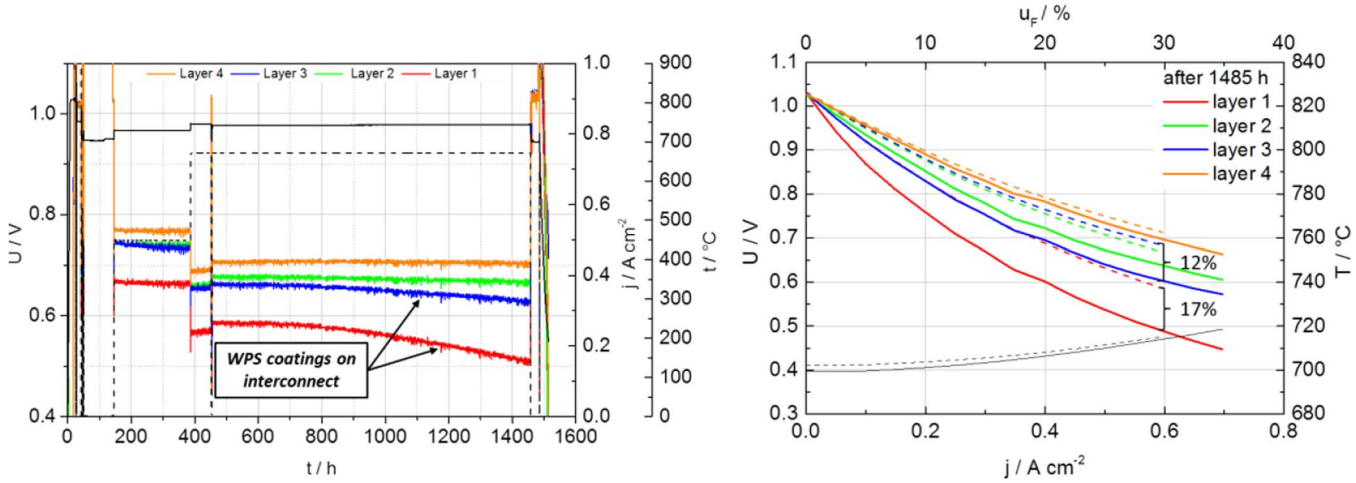

Figure 2. Comparison of the U-I curves before and after operation. Dashed lines represent the first curves at 700°C before load operation; solid lines the last measurement after 1485 h at 700°C before shutting down the stack.

Wet chemical etching.—The two different interconnect coatings not only result in different cell performance. Also the amount of Cr which is deposited in the cells after operation is quite different. For the layers with a dense MCF coating on the interconnect, the amounts of Cr measured (2.6–3.0 μg cm^{-2}) were, with respect to operating time and conditions, comparable to earlier results,[28] once again proving the high retention capability of these coatings.[15,34] For cells equipped with interconnects coated by wet-powder-sprayed MnO_x, the amount of Cr was considerably higher (114–160 μg cm^{-2}). It is interesting to note that the amount of Cr deposited in and on the cathode is in the same order of magnitude as that of a comparable stack operated for 17,000 h at 700°C and 0.5 A cm^{-2}, which could indicate a saturation effect.[35]

Microstructural results.—Because of the very low amount of Cr detected in layer 4, the main focus of this chapter is on the investigation of the layers equipped with WPS coatings on the interconnect. Fig. 3 shows a cross-sectional image of layer 1, a magnification of the LSCF/GDC/8YSZ interface, and the surface of the LSCF cathode.

From this, no obvious damage to the cell can be observed. The crack through the electrolyte is the result of shrinkage of the resin used for embedding the sample. Also the formation of a $SrZrO_3$ phase between the GDC diffusion barrier and the electrolyte (shown in the lower part of Fig. 3b) is always observed when functional layers fabricated by screen printing are used and is due to the high mobility of Sr. Its formation can be slowed down by using a denser GDC barrier layer applied by, for example, physical vapor deposition.[36,37] As expected for an LSCF cathode, the surface was covered with numerous Sr- and Cr-containing crystals. This is the most common location for the deposition of Cr species when using a mixed ionic-electronic conducting (MIEC) cathode such as LSCF.[25,27,35]

Investigating the cathode in greater detail revealed some deterioration in approximately the last 10 μm facing the GDC barrier layer. Compared to the upper bulk of the cathode, this area appears slightly fractured. This effect is present in every sample investigated with slightly varying intensity. Fig. 4 shows a comparison of the LSCF/GDC interface of layers 1 and 4 and a stack using the same internal construction and materials. This reference stack was operated for ∼1700 h at 700°C with a current density of 0.5 A cm^{-2}. The damage to the cathode is not present in the reference stack operated at lower current density.

In addition to the degradation of the microstructure in layer 1, the appearance of new phases can be observed. Fig. 5 shows the LSCF/GDC interface of layer 1 at higher magnification (highlighted by the red rectangle in Fig. 3).

It can be seen that small square crystallites have formed close to the GDC barrier layer. EDX point analysis was performed to obtain insights into the composition of these deposits. Fig. 6 shows two EDX spectra taken from the cross section of layer 1. One was taken from the bulk of the cathode, the other from a deposit at the LSCF/GDC interface. In the first spectrum, only the elements of the cathode material can be detected with quite similar intensities for La and Sr. In the second spectrum, this ratio changes noticeably toward higher Sr intensity. In addition, a significant Cr peak is present indicating the formation of a $SrCrO_x$ species.

Interestingly, neither in the bulk of the cathode nor in the upper region of the GDC was it possible to prove the presence of Cr. As already mentioned, the deposition of Cr at the electrochemically active area of the cell is rather rare when using a mixed ionic and electronic conducting LSCF cathode and, to our knowledge, has only been reported once before on the stack level.[28]

Discussion

At first sight, it seems as if the increase in current density triggered both the deterioration of the cathode and the deposition of a

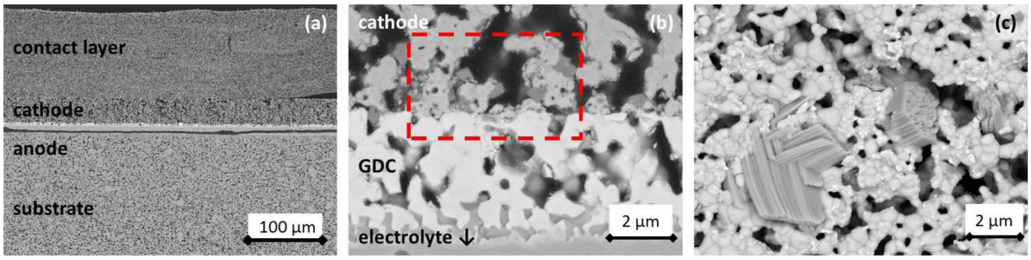

Figure 3. (a) SEM cross section of polished surfaces of layer 1; (b) LSCF/GDC interface of layer 1 showing the porosity of the GDC and the $SrZrO_3$ reaction zone beneath; (c) top view of LSCF cathode with $SrCrO_4$ crystals after operation (the crack in Fig 3a is due to sample preparation).

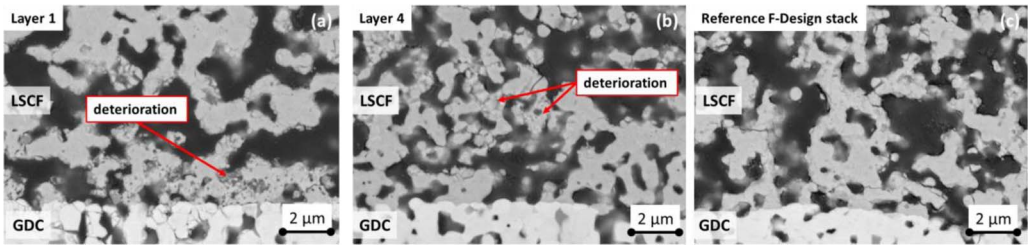

Figure 4. SEM cross section of the LSCF/GDC interfaces from (a) layer 1; (b) layer 4; (c) reference stack of the same design operated ~1700°C at 700°C with 0.5 A cm^{-2} without any obvious damage.

Cr-containing species at the LSCF/GDC interface. To obtain better insights into the degradation processes, we will separate the two effects, identify the general requirements and then discuss their interaction and plausibility.

Starting with cathode deterioration, it could be the result of a reduction in the LSCF at low oxygen partial pressure.[38,39] During operation, the $p(O_2)$ inside the cathode layer is a function of a variety of parameters, e. g. the cathode feed volume flux, the porosity of the layer, and the current density. From stacks operated in JÜLICH, we expect the cathode material to display long-term stability at current densities of up to 0.5 A cm^{-2} at temperatures between 700–800°C, without showing any deterioration as is presented in the SEM section (Fig. 4c).[40]

According to Kuhn et al., stoichiometric LSCF6428 ($(La_{0.60}Sr_{0.40})(Co_{0.20}Fe_{0.80})O_{3-\delta}$) starts to decompose at an $p(O_2)$ of 1E-8 bar.[41] However, it is at least questionable whether the local oxygen partial pressure in the electrochemically active area of the cathode drops by seven orders of magnitude (using 2.1E-1 bar in air as starting point) and so far little is known about the long-term stability of LSCF at moderately low oxygen partial pressures under realistic operating conditions including both temperature and current. As the $p(O_2)$ at the LSCF/GDC interface cannot be measured during operation, it was calculated using the finite element method (FEM) model from Geisler et al.[42,43] According to the simulation results, the oxygen partial pressure under the channels of the interconnect decreases by roughly 50% from 0.21 bar when the stack is operated at 0.75 A cm^{-2}. Below the ribs of the interconnect, an even more severe pO_2 decrease of up to several orders of magnitude can be expected, depending on the microstructural properties and thickness of the cathode contact layer and cathode. It has to be pointed out that the simulations conducted so far are based on CCL parameters derived from SEM imaging to fit the characteristics of this stack, and therefore have potential for improvement and refinement, e.g. by extracting cell properties from focused ion beam-scanning electron microscopy (FIB-SEM) tomography. An additional factor not addressed by the model so far is the Cr surface reaction as shown in Fig. 3c. Deposits on the surface of the cathode will hinder oxygen transportation to the electrochemically active sites. As a result, the local $p(O_2)$ will decrease, which then influences Cr deposition and the stability of the LSCF. Based on these first results, it seems quite unlikely that the deterioration is caused by an extremely low oxygen partial pressure, which, according to the literature, is necessary to chemically reduce LSCF.[41]

What seems more likely is a slight fracturing of the cathode due to chemical expansion, which does not require extremely low oxygen partial pressure but rather a sufficient amount of time. According to Bouwmeester et al., the ionic conductivity of stoichiometric LSCF6428 is correlated to the oxygen partial pressure. In the temperature range of 600–800°C below an oxygen partial pressure of approximately 1E-2 bar, the oxygen vacancies formed in the LSCF start to interact with each other, thereby decreasing the ionic conductivity. Furthermore, a high concentration of oxygen vacancies, which is localized to a limited volume of the cathode, changes the lattice parameters in the respective area and thereby introduces mechanical stress. A sufficiently strong gradient might trigger processes such as kinetic demixing, decomposition and finally failure.[44] This is in good agreement with the studies by Endler-Schuck et al., who showed that the time-dependent performance degradation of porous LSCF cathodes in single cell measurements is correlated to a loss in oxygen ion bulk diffusion.[45,46] Based on the SEM analysis conducted in the present work, it cannot be conclusively determined whether the cathode was damaged due to an extremely low $p(O_2)$ or due to a combination of a moderately decreased $p(O_2)$ and the intrinsic degradation of the LSCF material itself. The fact that only a slight microstructural

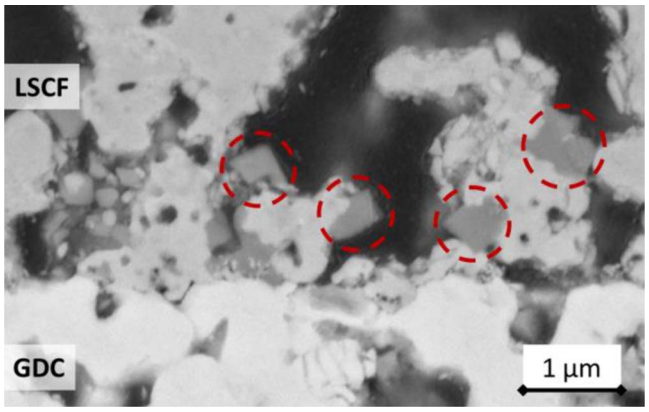

Figure 5. Higher magnification SEM of the LSCF/GDC interface of layer 1. Highlighted: formation of small crystallites not present before stack operation.

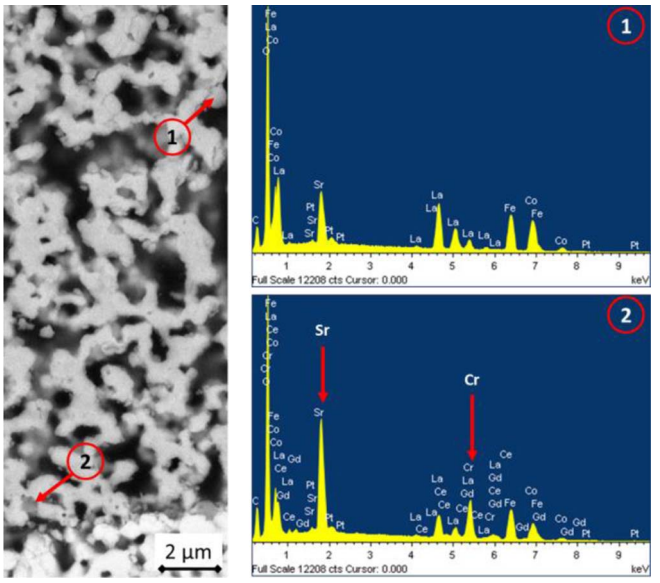

Figure 6. Excerpt from the EDX analysis comparing the bulk of the cathode and a deposit at the LSCF/GDC interface.

degradation was observed points to an environment which is close to the stability limit of the LSCF cathode. A much longer operating time would have been necessary for complete failure of the cathode.

With respect to Cr poisoning, the basic requirement for the reaction between a volatile Cr species and an LSCF cathode is the availability of SrO, which segregates from the perovskite lattice to the surface. Since it is expected that the SrO will be available on the entire cathode, including inner surfaces such as pores, a gradient of Cr from the surface of the cathode down to the GDC barrier layer seems most likely. To assess the reaction of gaseous Cr species with SrO on the cathode, calculations based on the SGPS database using FactSage[47] were performed. For this purpose, the most likely reactions between solid SrO and gaseous Cr species (3–5) are compared in terms of their Gibb's free energy ΔG. CrO_3 is considered to be the dominant Cr species in the gas phase, because the stack was operated with dry air on the cathode side.[8]

$$SrO(s) + CrO_3(g) \rightarrow SrCrO_4(s) \quad [3]$$

$$SrO(s) + \frac{2}{3}CrO_3(g) \rightarrow \frac{1}{3}Sr_3Cr_2O_8(s) + \frac{1}{6}O_2(g) \quad [4]$$

$$SrO(s) + \frac{1}{2}CrO_3(g) \rightarrow \frac{1}{2}Sr_2CrO_4(s) + \frac{1}{4}O_2(g) \quad [5]$$

The calculations were performed with respect to the elevated operating temperature at high current density in the range of 700°C to 750°C and 1 bar absolute pressure. Fig. 7a shows a diagram of the isothermal predominance area diagram, which indicates the dominant (most stable) reaction product as a function of $p(O_2)$ (X-axis) and $p(CrO_3)$ (Y-axis).

The starting $p(O_2)$ is set to 2.1E-1 bar by the use of air as the cathode feed. The Cr partial pressure is a function of many different parameters and can only be estimated based on reasonable assumptions. In dry air, the equilibrium Cr partial pressure above pure Cr_2O_3 is in the range of 1E-10 bar.[11] However, the Cr evaporation is highly dependent on the Cr source. While it is highest for the pure oxide, it is much lower for a Crofer22APU steel, which forms a (Cr,Mn)-spinel phase on its own, thereby reducing Cr evaporation.[32] Additionally, the interconnects used in the present study were coated with an APS MCF or a WPS MnO_x protection layer. Therefore the Cr partial pressure on the cathode side is expected to be many orders of magnitude lower than the saturation value of Cr_2O_3 at 700°C. The most appropriate way to interpret the results from the FactSage calculation is to follow the cathode feed flux. Starting in the cathode compartment ① in Figs. 7a and 7b, CrO_3 will react with SrO on the cathode surface forming $SrCrO_4$ crystallites. Due to this reaction, the Cr partial pressure of the air that enters the cathode decreases. At a critical Cr partial pressure, the Gibbs free energy for the reaction between CrO_3 and SrO shifts to positive values and the reaction is no longer favorable (② in Figs. 7a and 7b). This is expected to take place in the bulk of the cathode, where a huge inner surface of the LSCF with segregated SrO is available to getter the last traces of Cr from the gas phase. Due to the low Cr partial pressure and the huge surface available, the minor Cr-containing deposits are much too small to be detected using SEM/EDX. The electrochemical activity of the cathode is highest in the last few µm of the LSCF cathode facing the GDC barrier layer. The processes in this area are shown schematically in Fig. 7c. Due to the reduction of oxygen, the local oxygen partial pressure in this area of the cathode decreases, resulting in a shift of the equilibrium for the reaction between the gaseous Cr species and the SrO on the LSCF surface, indicated by the dashed red arrow in Fig. 7a. Depending on the final oxygen partial pressure, the Cr-consuming reaction can restart but will now occur according to 4 or 5.

Finally, the influence of the temperature should be discussed. As the stack was equipped with only one thermocouple in the middle of the interconnect between layer 2 and 3, there is no information about the real temperature distribution in the investigated stack. However, the characteristic temperature distribution is available from a comparable

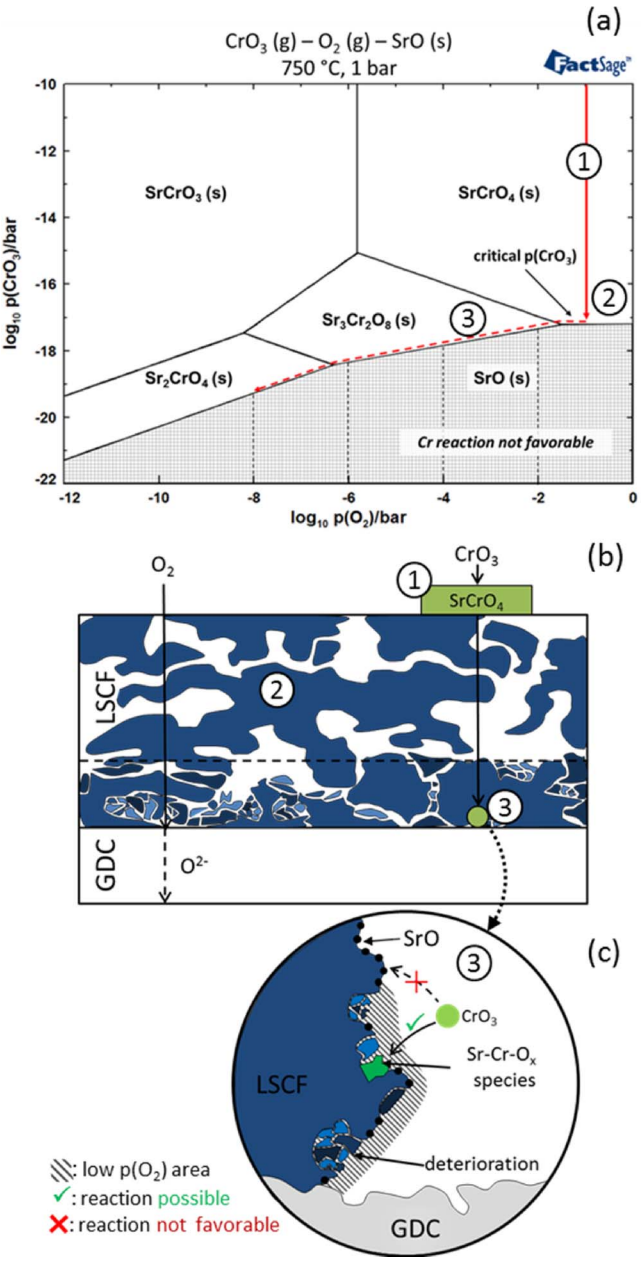

Figure 7. (a) Isothermal predominance diagram of the reaction between CrO_3 and SrO as a function of $p(CrO_3)$ and $p(O_2)$. (b) & (c): Scheme of the corresponding reactions. ① Surface reaction and decrease of $p(CrO_3)$, ② reaction in the bulk phase not favorable, ③ reaction at the LSCF/GDC interface and deterioration of the LSCF due to low $p(O_2)$.

four-layer stack equipped with nine thermocouples. This reference stack was operated at 700°C and 0.5 A cm^{-2}. In Fig. 8, the temperature profile of this stack, a schematic cross section and the temperature dependence of the Cr reaction is shown.

As expected, the temperature distribution of the bottom layer differs considerably from the layers above, showing the maximum temperature at the air outlet and a steady decrease toward the inlet. For the two other layers, the maximum temperature is measured in the middle of the layer. Due to the small stack size and the moderate fuel utilization, the temperature gradient for the upper two layers is in the range of only 5 K and 10 K for the bottom layer, respectively. Adapting this temperature profile to the stack investigated in this study, it is found to be in good agreement with the results of the microstructural analysis and the FactSage calculations. According to Fig. 8c,

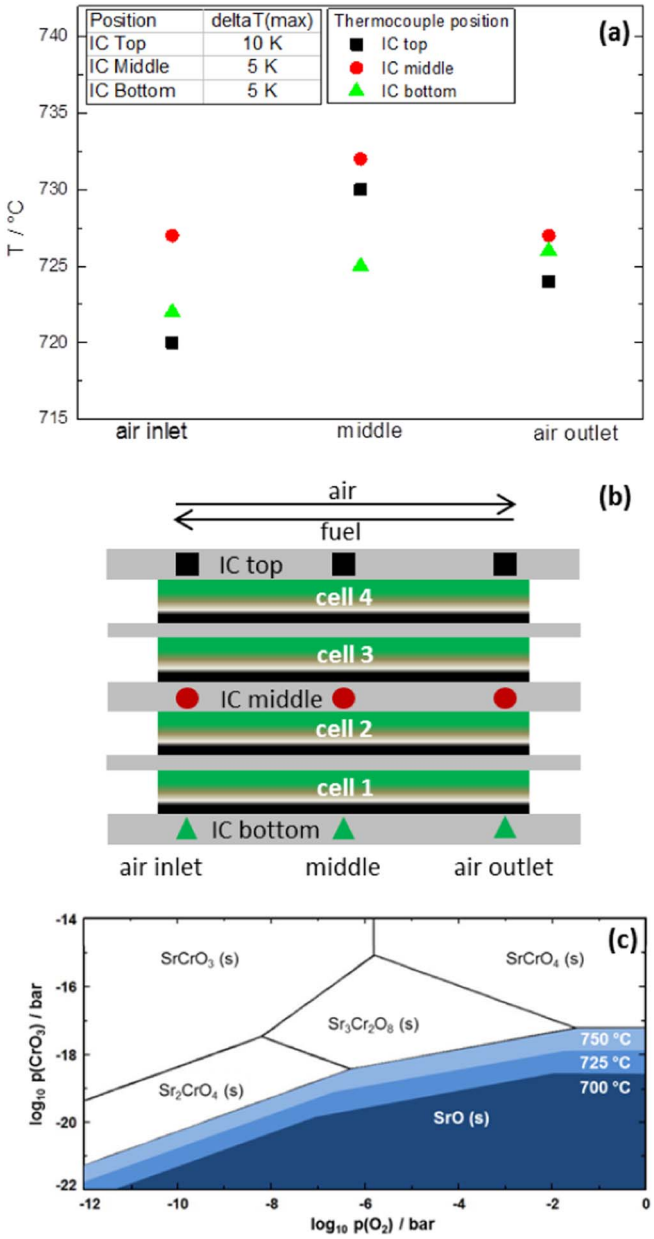

Figure 8. (a) Schematic temperature distribution of a comparable short stack equipped with 9 thermocouples (fuel inlet/middle/fuel outlet) operated at 700°C and 0.5 A cm^{-2}; (b) stack scheme; (c) temperature shift of the critical p(CrO_3) with increasing temperature. (IC = interconnect).

the critical Cr partial pressure, where the reaction between SrO and CrO_3 stops, increases with increasing temperature. Therefore the low temperature at the air inlet of layer 1 favors the deposition of Cr at the LSCF/GDC interface. The investigation of layer 3, which should have had the lowest temperature gradient but the highest absolute cell temperature during operation, revealed fewer/smaller Cr depositions at the LSCF/GDC interface and a comparable deterioration.

Finally, it should be mentioned that this is just the first step in understanding the underlying mechanism of Cr degradation under high load conditions. In particular, the influence of the temperature and the current distribution are difficult to assess in a stack test and therefore require a more sophisticated test setup than used for this study.

Conclusions

Anode-supported solid oxide fuel cells were tested in a four-layer JÜLICH F-design stack. Two layers were equipped with interconnects coated by dense atmospheric plasma-sprayed (APS) manganese-cobalt-iron-spinel (MFC) layers, the other two were coated with a porous wet-powder-sprayed (WPS) manganese oxide (MnO_x) coating. The stack was operated for 240 h at 700°C at a current density of 0.5 A cm^{-2} and at 0.75 A cm^{-2} for a further 1000 h. During operation, the layers with WPS coatings showed significantly higher degradation compared to those with APS coatings. In the post mortem analysis, significant amounts of Cr were detected in the layers with WPS interconnect coatings. Sr- and Cr-containing crystals with a size of several µm were observed on the surface of these layers using SEM and small deposits of a Cr-containing species were identified adjacent to the LSCF/GDC interface. Regardless of the interconnect coating, in all the investigated layers a deterioration of the cathode close to the LSCF/GDC interface was found.

To explain the analytical findings, isothermal predominance area diagrams of the SrO-CrO_3-O_2 system were calculated using FactSage. The results show that the reaction between the gaseous Cr species and the SrO formed by Sr segregation from the cathode material is highly dependent on the p(CrO_3) and p(O_2). If both are sufficiently high, $SrCrO_4$ will be formed, as observed on the cathode surface. A deposition at the LSCF/GDC interface can be triggered by very low partial pressures for both species. In addition, a decreased p(O_2) may be responsible for the slight fracturing of the cathode, as LSCF is not intended to have long-term stability under reducing conditions. As neither of these effects was observed in comparable stacks operated at current densities of up to 0.5 A cm^{-2} the 50% higher current density and the temperature increase thus induced seems to be the driving force for Cr deposition and cathode damage.

In conclusion, this study contributes a new aspect to the investigation of the Cr-related degradation of SOFCs. Operating parameters such as current density and temperature have a significant influence on the interaction between an LSCF cathode and gaseous Cr species. However, more investigations are necessary to understand the underlying mechanisms completely. So far the theory developed here is mainly supported by empirical findings and earlier stack tests conducted at lower current density which did not show deterioration or Cr deposition at the LSCF/GDC interface. Starting from the results presented here, a logical progression is to investigate the actual conditions at the LSCF/GDC interface in more detail, e. g. by FEM modeling based on data derived from FIB-SEM tomography. By using parameters and data obtained from a real system, such an approach could provide important insights into oxygen transportation and the resulting atmosphere as a function of the operating conditions and microstructural changes.

Acknowledgments

Christian Doppler Laboratories are funded in equal shares by the public authorities and the companies directly involved in the laboratories. The financial support by the Austrian Federal Ministry of Science, Research and Economy and the National Foundation for Research, Technology and Development is gratefully acknowledged. Moreover, the authors thank the industrial project partners Plansee SE and AVL List GmbH, Dr. D. Sebold (IEK-1) for SEM imaging, U. de Haart (IEK-3) for performing the stack tests, and H. Geisler for FEM simulation (KIT IAM-WET).

References

1. A. B. Stambouli and E. Traversa, *Renewable and Sustainable Energy Reviews*, **6**, 433 (2002).
2. M. C. Tucker, *Journal of Power Sources*, **195**, 4570 (2010).
3. N. H. Menzler, A. Mai, and D. Stöver, in *Handbook of Fuel Cells*, W. Vielstich, A. Lamm, H. A. Gasteiger, and H. Yokokawa Editors, John Wiley & Sons, Ltd, Chichester, UK (2010).

4. M. Haydn, K. Ortner, T. Franco, S. Uhlenbruck, N. H. Menzler, D. Stöver, G. Bräuer, A. Venskutonis, L. S. Sigl, H. P. Buchkremer, and R. Vaßen, *Journal of Power Sources*, **256**, 52 (2014).
5. D. J. L. Brett, A. Atkinson, N. P. Brandon, and S. J. Skinner, *Chemical Society reviews*, **37**, 1568 (2008).
6. S. Badwal, R. Deller, K. Foger, Y. Ramprakash, and J. Zhang, *Solid State Ionics*, **99**, 297 (1997).
7. M. C. Tucker, H. Kurokawa, C. P. Jacobson, L. C. De Jonghe, and S. J. Visco, *Journal of Power Sources*, **160**, 130 (2006).
8. K. Hilpert, *Journal of The Electrochemical Society*, **143**, 3642 (1996).
9. S. P. Jiang, S. Zhang, and Y. Zhen, *Journal of The Electrochemical Society*, **153**, A127 (2006).
10. C. C. Wang, T. Becker, K. Chen, L. Zhao, B. Wei, and S. P. Jiang, *Electrochimica Acta*, **139**, 173 (2014).
11. X. Chen, P. Hou, C. Jacobson, S. Visco, and L. Dejonghe, *Solid State Ionics*, **176**, 425 (2005).
12. M. Stanislowski, J. Froitzheim, L. Niewolak, W. J. Quadakkers, K. Hilpert, T. Markus, and L. Singheiser, *Journal of Power Sources*, **164**, 578 (2007).
13. M. J. G. Vargas, M. Zahid, F. Tietz, and A. Aslanides, in *10th International Symposium on Solid Oxide Fuel Cells (SOFC-X)*, p. 2399 (2007).
14. J. Malzbender, P. Batfalsky, R. Vaßen, V. Shemet, and F. Tietz, *Journal of Power Sources*, **201**, 196 (2012).
15. L. Blum, L. G. J. d. Haart, J. Malzbender, N. H. Menzler, J. Remmel, and R. Steinberger-Wilckens, *Journal of Power Sources*, **241**, 477 (2013).
16. R. Vaßen, N. Grünwald, D. Marcano, N. H. Menzler, R. Mücke, D. Sebold, Y. J. Sohn, and O. Guillon, *Surface and Coatings Technology*, **291**, 115 (2016).
17. S. P. Simner, M. D. Anderson, M. H. Engelhard, and J. W. Stevenson, *Electrochemical and Solid-State Letters*, **9**, A478 (2006).
18. M. Finsterbusch, A. Lussier, J. A. Schaefer, and Y. U. Idzerda, *Solid State Ionics*, **212**, 77 (2012).
19. W. Lee, Z. Cai, and B. Yildiz, *ECS Transactions*, **45**, 405 (2012).
20. G. M. Rupp, H. Téllez, J. Druce, A. Limbeck, T. Ishihara, J. Kilner, and J. Fleig, *J. Mater. Chem. A*, **3**, 22759 (2015).
21. K. Szot and W. Speier, *Physical Review B*, **60**, 5909 (1999).
22. H. Ding, A. V. Virkar, M. Liu, and F. Liu, *Physical chemistry chemical physics: PCCP*, **15**, 489 (2013).
23. E. J. Crumlin, E. Mutoro, Z. Liu, M. E. Grass, M. D. Biegalski, Y. -L. Lee, D. Morgan, H. M. Christen, H. Bluhm, and Y. Shao-Horn, *Energy & Environmental Science*, **5**, 6081 (2012).
24. E. Konysheva, H. Penkalla, E. Wessel, J. Mertens, U. Seeling, L. Singheiser, and K. Hilpert, *Journal of The Electrochemical Society*, **153**, A765 (2006).
25. L. Zhao, J. Drennan, C. Kong, S. Amarasinghe, and S. P. Jiang, *Journal of Materials Chemistry A*, **2**, 11114 (2014).
26. Y. Matsuzaki and I. Yasuda, *Journal of The Electrochemical Society*, **148**, A126 (2001).
27. E. Konysheva, *Russian Journal of Electrochemistry*, **50**, 630 (2014).
28. N. H. Menzler, D. Sebold, and E. Wessel, *Journal of Power Sources*, **254**, 148 (2014).
29. S. M. Gross, D. Federmann, J. Remmel, and M. Pap, *Journal of Power Sources*, **196**, 7338 (2011).
30. M. Stanislowski, E. Wessel, K. Hilpert, T. Markus, and L. Singheiser, *Journal of The Electrochemical Society*, **154**, A295 (2007).
31. R. Trebbels, T. Markus, and L. Singheiser, *ECS Transactions*, **25**, 1417 (2009).
32. R. Trebbels, T. Markus, and L. Singheiser, *Journal of Fuel Cell Science and Technology*, **7**, 011013 (2010).
33. P. Batfalsky, J. Malzbender, and N. H. Menzler, *International Journal of Hydrogen Energy*, **41**, 11399 (2016).
34. L. Blum, P. Batfalsky, Q. Fang, L. G. J. de Haart, J. Malzbender, N. Margaritis, N. H. Menzler, and R. Peters, *Journal of The Electrochemical Society*, **162**, F1199 (2015).
35. N. H. Menzler, P. Batfalsky, S. M. Gross, V. Shemet, and F. Tietz, in *219th ECS Meeting*, p. 195, ECS (2011).
36. S. Uhlenbruck, T. Moskalewicz, N. Jordan, H. J. Penkalla, and H. P. Buchkremer, *Solid State Ionics*, **180**, 418 (2009).
37. M. Z. Khan, R. -H. Song, S. -B. Lee, J. -W. Lee, T. -H. Lim, and S. -J. Park, *International Journal of Hydrogen Energy*, **39**, 20799 (2014).
38. M. H. R. Lankhorst and J. E. t. Elshof, *Journal of Solid State Chemistry*, **130**, 302 (1997).
39. S. -i. Hashimoto, Y. Fukuda, M. Kuhn, K. Sato, K. Yashiro, and J. Mizusaki, *Solid State Ionics*, **181**, 1713 (2010).
40. L. Blum, L. G. J. de Haart, J. Malzbender, N. Margaritis, and N. H. Menzler, *Energy Technology*, **4**, 939 (2016).
41. M. Kuhn, Y. Fukuda, S. Hashimoto, K. Sato, K. Yashiro, and J. Mizusaki, in *219th ECS Meeting*, p. 1881, ECS (2011).
42. H. Geisler, A. Kromp, A. Weber, and E. Ivers-Tiffee, *Journal of the Electrochemical Society*, **161**, F778 (2014).
43. H. Geisler, A. Kromp, J. Joos, A. Weber, and E. Ivers-Tiffee, *ECS Transactions*, **68**, 3043 (2015).
44. H. J. M. Bouwmeester, M. W. Den Otter, and B. A. Boukamp, *Journal of Solid State Electrochemistry*, **8**, 599 (2004).
45. C. Endler, A. Leonide, B. Rüger, A. Weber, and E. Ivers-Tiffée, in *217th ECS Meeting*, p. 71, ECS (2010).
46. C. Endler-Schuck, J. Joos, C. Niedrig, A. Weber, and E. Ivers-Tiffée, *Solid State Ionics*, **269**, 67 (2015).
47. C. W. Bale, E. Bélisle, P. Chartrand, S. A. Decterov, G. Eriksson, A. E. Gheribi, K. Hack, I. -H. Jung, Y. -B. Kang, J. Melançon, A. D. Pelton, S. Petersen, C. Robelin, J. Sangster, P. Spencer, and M. -A. van Ende, *Calphad*, **54**, 35 (2016).